nature electronics

ARTICLES

https://doi.org/10.1038/s41928-021-00663-0

Check for updates

Textile-integrated metamaterials for near-field multibody area networks

Amirhossein Hajiaghajani[1], Amir Hosein Afandizadeh Zargari[1,2], Manik Dautta[1], Abel Jimenez[1], Fadi Kurdahi[1,2] and Peter Tseng[1,3] ✉

Wearable and implantable sensors can be linked together to create multi-node wireless networks that could be of use in the development of advanced healthcare monitoring technologies. Such body area networks require secure, seamless and versatile communication links that can operate across the complex human body, but they typically suffer from short ranges, low power or the need for direct-connection terminals. Here we show that textile-integrated metamaterials can be used to drive long-distance near-field communication (NFC)-based magneto-inductive waves along and between multiple objects. The metamaterials are built from arrays of discrete, anisotropic magneto-inductive elements, creating a mechanically flexible system capable of battery-free communication among NFC-enabled devices that are placed anywhere close to the network. Our approach offers a secure and on-demand body area network that has the potential for straightforward expansion and can span across different pieces of clothing, objects and people.

Health monitoring and activity tracking technologies rely on wearable or implantable sensors that link to different regions of the human body (or, in fact, multiple bodies). These sensors can be used to create multi-node networks that interpret information from our body and the objects that interact with it. To parse biometric information in real time, such networks require secure and reliable communication links between the nodes[1,2]. These links are generally known as body area networks (BANs). The robustness of a BAN is dependent on a number of characteristics: the level of comfort (or the size/weight of the device nodes), adaptability to pre-existing clothing, compliance with commonly used standards[3], node sampling rates and wireless powering capabilities[4]. It is also dependent on the ability to communicate with nearby BANs and local area networks, creating a seamless connection with peripheral Internet of Things technology without compromising on security. Ideally, a BAN can offer such communication capabilities in addition to being lightweight and battery free (to minimize user burden and facilitate continuous monitoring), as well as being capable of sampling dynamically placed wireless nodes at high rates relevant to the unpredictability of daily lives.

BANs have traditionally been equipped with over-the-air communications including custom radio-frequency (RF) transducers[5], RF identification[6] or Bluetooth[7]. However, such radiative approaches often suffer from high power consumption and relatively low levels of security. This is because despite the coding methods, a nearby third-party receiver may listen to the communication between the reader or sensing nodes. This issue can be addressed by limiting the operational range of such communication links to ensure the target receiver/transmitters are placed spatially close enough to the body. One hardware solution to this challenge is to convert/replace the far-field radiation unit (such as the planar inverted-F antenna in Bluetooth technology) with a near-field antenna[8] and employ surface waves (instead of spatial radiation). This, however, requires exclusively developed Bluetooth sensors as well as a modified reader (often a mobile phone) with irregular antennas, which limits wider application. In addition, Bluetooth power transfer is limited and batteries are typically required at the sensing nodes to accurately sample the environment.

Based on Bluetooth technology, a surface-plasmon-like metamaterial network made out of laser-cut conductive fabrics and attached on clothing with a textile adhesive has been recently introduced, offering surface-bound magnetic-wave propagation at 2.4 GHz [8–10]. However, such networks must exhibit continuous conductivity across their entire length scale (otherwise, substantial transmission loss occurs) and require relatively complex sewing steps to attach onto clothing. The electrical characteristics of these BANs at microwave frequencies also exhibit rather large sensitivity to the presence of tissues and environmental changes. In addition, the BAN architectures, which have continuous conductivity across the array, cannot be readily reconfigured onto pre-existing clothing and suffer from difficult clothing attachment methods, thus limiting their practical utility and making network expansion difficult. Furthermore, the embroidered spoof surface plasmon metamaterials are not suitable for use below gigahertz frequencies, as they would require larger dimensions at lower frequencies (for near-field communication (NFC)). Moreover, the enhanced security enabled by redirecting the transmitted energy to guided modes (instead of conventional long-range far-field radiation) does not allow third-party devices to listen to Bluetooth communication. This redirection is not often fully efficient, resulting in power leakage at microwave frequencies and ultimately challenging the signal transmission. Although custom Bluetooth antennas with near-field emission profiles are available, they are not currently used in commercial Bluetooth sensors and/or readers and may violate relevant regulation standards. Finally, in such spoof surface plasmon structures, the wave propagates on and very close to the surface, which limits propagation from object to object[11] that could occur between pieces of clothing or nearby BANs.

Another approach to enhance BAN security, which does not require alteration from relevant standards, is to use near-field emitting devices such as NFC or Qi-based technologies. A single reader can use several near-field emitting hot spots (that are

[1]Department of Electrical Engineering and Computer Science, University of California, Irvine, CA, USA. [2]Center for Embedded and Cyber-physical Systems, University of California, Irvine, CA, USA. [3]Department of Biomedical Engineering, University of California, Irvine, CA, USA. ✉e-mail: tsengpc@uci.edu

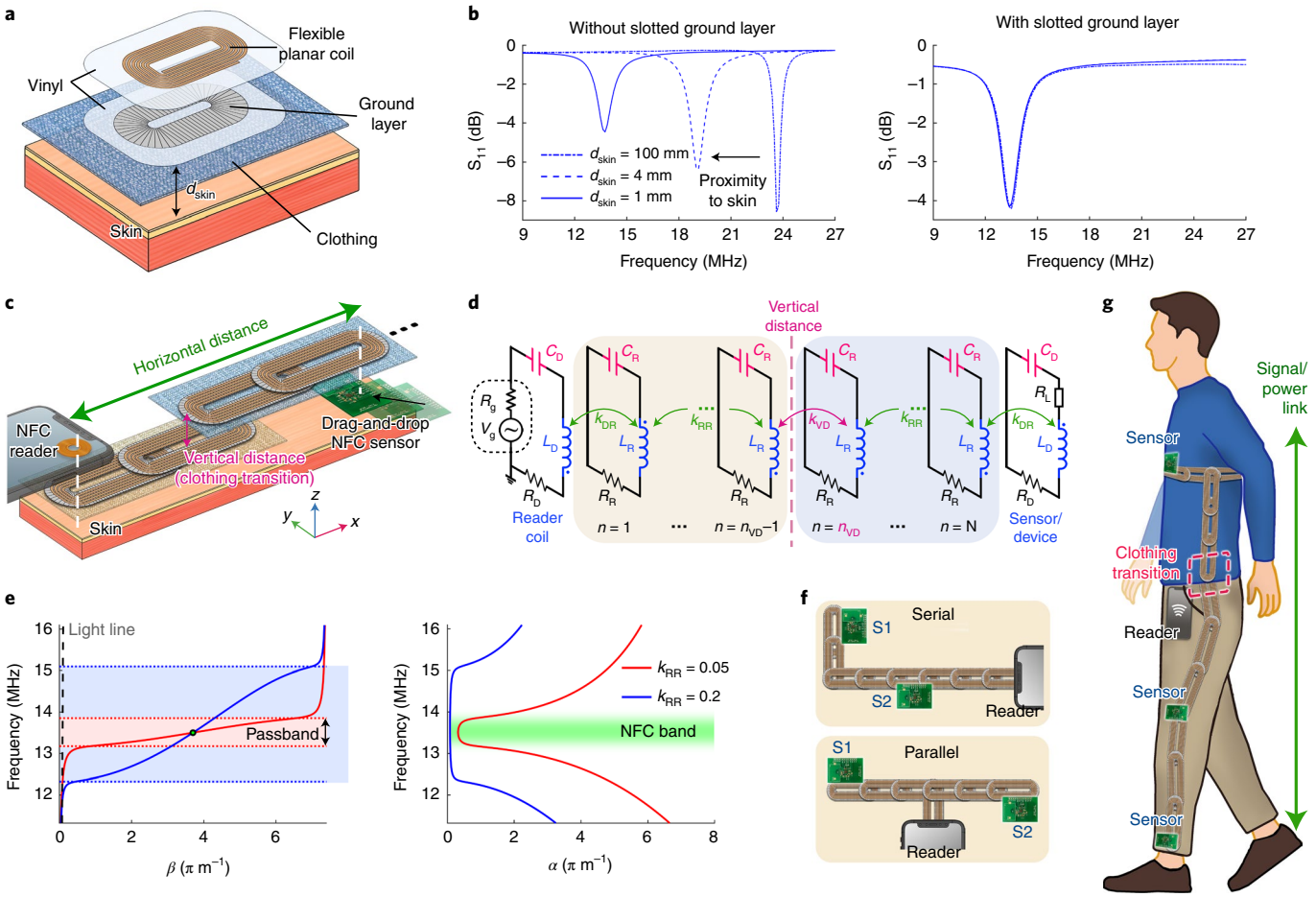

Fig. 1 | Design of textile-integrated metamaterials for magneto-inductive wave propagation. a, Blow-up schematic of a flexible, planar magnetic resonator. **b**, The ground layer minimizes spectral uncertainty due to the human body's parasitic effect. **c**, NFC sensors can be dragged and dropped across the magnetically coupled resonators with a horizontal distance (in the *x* direction) and a vertical distance in other directions. **d**, Equivalent circuit of the magneto-inductive metamaterial with potential object-to-object transitions (at the n_{VD}th resonator). **e**, Dispersion diagram for the array of resonators for various magnetic coupling coefficients. The lower and higher cut-off frequencies (magneto-inductive-wave passband) are marked by dotted lines and specify the bandwidth. The light line (with a large slope of the light velocity in free space) is shown by the dashed line. **f**, Reader and multiple sensors can be utilized in an inline serial or T-shaped parallel array of resonators to form various signal paths around the body. **g**, Metamaterial network is easily streamlined into separate clothing pieces, enabling the high flexibility necessary for daily routines and significant extension of the horizontal range. The nodes may be placed anywhere close to (within a few centimetres of) any point of the network.

connected by a wire) to transmit signals to often battery-free wireless nodes placed around the body[12–15]. An advantage of NFC over the Bluetooth protocol is its plug-and-play ability to seamlessly pair communication nodes to the reader, in addition to supporting wireless power transfer. This enables pick-and-place characteristics that allow wireless sensing nodes to be switched at will. Such capabilities should reduce user burden and increase convenience in day-to-day use.

With the near-field regime, research has focused on connecting a few loop antennas (known as hubs and terminals) using embroidered conductive thread[12,14] or metal wires[13]. In such structures, the NFC transponders can pair only if placed close to these static hot spots. The wire-linked nature of this approach also makes it unsuitable for on-demand expansion due to long wires used to connect the disparate terminals. Although wireless, wearable inter-coil communication has been shown to connect two wristband-like coils[16], it suffers from a short operational range[17,18]. Similarly, the low-frequency capacitive signalling of human skin and muscle[19] can impede the powering of battery-free sensor nodes and may be easily disrupted by or interfere with immediate surroundings (particularly, conductive substances).

Electromagnetic surface-wave propagation (often achieved via metamaterials) operating at low-frequency bands could potentially be used to create an extendable and wireless BAN in NFC bands. Electromagnetic metamaterials typically function at relatively large frequencies (above the gigahertz range) and are fabricated in rigid forms to ensure their perfectly periodic structure. Magneto-inductive (also known as magnetic metamaterials) structures have, in particular, been shown to allow wave propagation[20–25], enabling a communication path bounded to an array of magnetically coupled resonators (conventionally, an array of split rings). Their utility ranges from high-frequency metasurface applications[26] to wireless power transfer[27–29]. Due to the magnetically coupled nature of such resonators, and unlike spoof surface plasmon structures, magneto-inductive arrays are wirelessly connected. Magneto-inductive structures with three-dimensional coaxial and in-plane magnetically coupled rings also offer some degree of bending for the powering path[20,27,30,31]. However, they have not previously had enough mechanical flexibility to support human motion, and are difficult to synthesize and scale to large/curvy structures.

In this Article, we report the development of metamaterial textiles that can be added to pre-existing clothing to create drag-and-drop

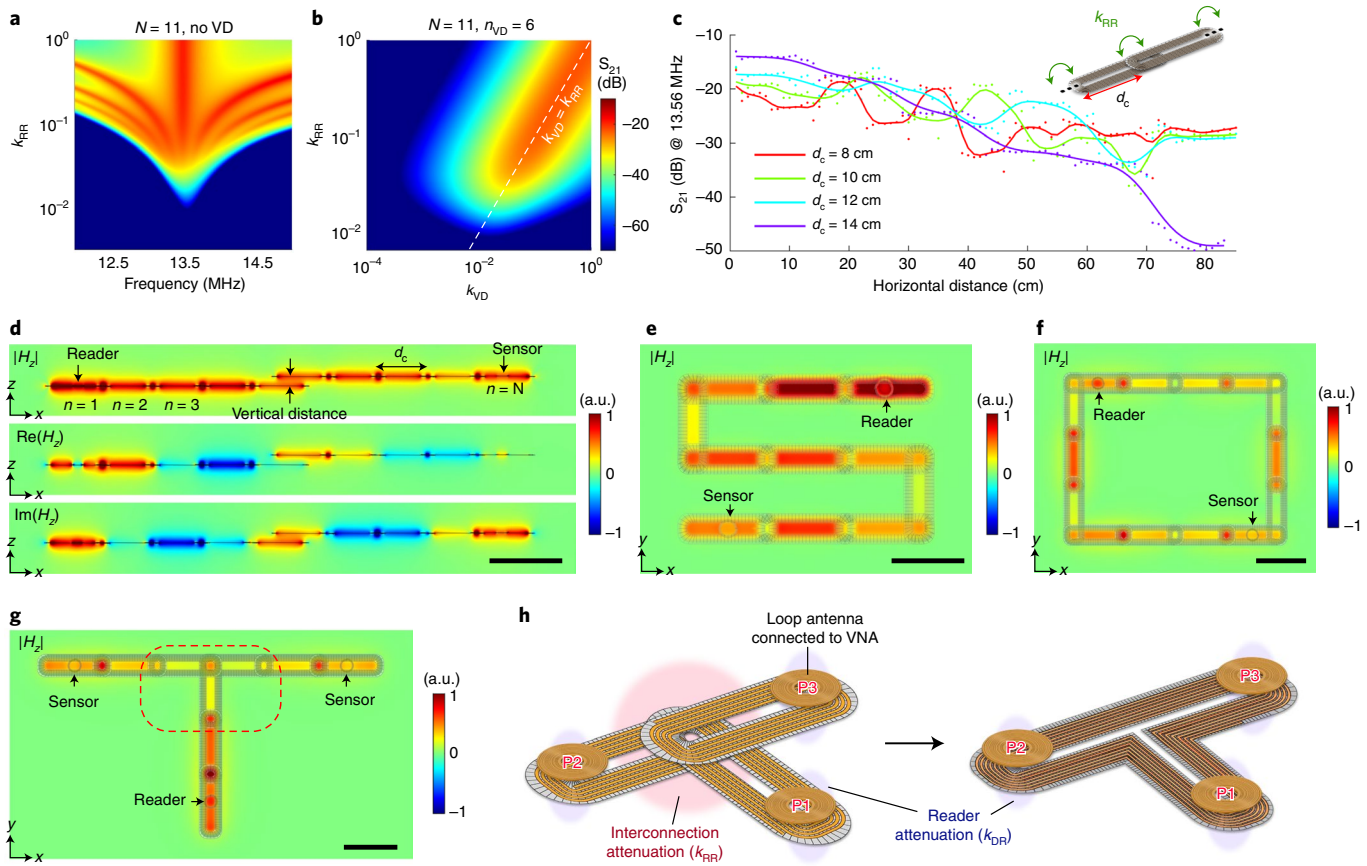

Fig. 2 | Wave propagation along complex pathways of magnetic metamaterials. a, The transmission profile of an inline network of resonators for varying inter-coil coupling (coil distancing). **b**, The transmission profile for inter-coil (horizontal) coupling versus a coupling anomaly generated by a vertical distance (VD) in the middle of the network. **c**, The experimentally measured $|S_{21}|$ over an inline array of resonators for various coil distancings (without VD), demonstrating the artificially created standing wave along the magneto-inductive waveguide. **d**, Side view of the perpendicular magnetic field (H_z) distribution showing the standing wave (at $\beta d_c \approx \pi/2$) along the inline resonator path with 2 cm of vertical distance in between. **e**–**g**, Top view of the magnetic field of meandered S-shaped (**e**), circular (**f**) and branched T-shaped (**g**) pathways. **h**, Multiple coils (P1–P3) sharing the intersection can be merged into one piece to lower the system loss by reducing the number of interconnections, thus enhancing the transmission profile. VNA, vector network analyser (all scale bars, 10 cm).

near-field multiple BANs. We use flexible magneto-inductive elements that are tuned to the NFC band[32] and support the picking and placing of wireless nodes along the network. Inspired by modern low-cost vinyl clothing production, our approach to integrate magneto-inductive networks on textiles eliminates the need for complicated sewing techniques and the relatively expensive conductive threads necessary in such methods. This network can be designed, built and expanded at will to fit user needs. The magneto-inductive elements are composed of discrete, planar and flexible microelectronics-free loops, with spectral behaviour that is stabilized against human body effects[3,33,34]. They, thus, create a tunable power/communication path across the human body. This is achieved by internally bounding the electric fields (which are easily perturbed by human body effects) within the structure and utilizing quasi-static magnetic fields. A time-division multiple access protocol was also implemented to interrogate multiple NFC-enabled sensors connected across the body through discrete pieces of clothing.

Our approach creates a secure on-demand BAN, whose communication link can span across different pieces of clothing, objects or people. The battery-free, energy-harvesting transponders used in this system reduce user burden, allow continuous monitoring and minimize node size (via battery elimination and memory reduction). The approach could lead to self-sustained, zero-battery BAN ecosystems with cloud assistance[35–37].

Network design and analysis

Magneto-inductive waves propagate through an array of magnetically coupled resonant structures that possess equivalent spectral characteristics as metamaterials. The resonators can be designed in different forms depending on the network's desired characteristics. Traditionally, they are created with rigid loops whose impedance is tuned by lumped elements[38]. In our approach, the requirements of BANs impose a narrow set of constraints on the performance of the magneto-inductive waveguide, as it must exhibit high degrees of flexibility, be insensitive to bodily motion, be easy to extend and possess a microelectronics-free design. We design multi-turn flexible planar coils made of metal (aluminium and/or copper) foils as resonators to be integrated into the clothing textile. The resonance characteristic of such coils, however, highly depends on the undesired parasitic capacitances between the coil and human body. This may interfere with magneto-inductive wave propagation as the textile-integrated network is not fixed on the body and the distance from the skin (d_{skin}) moves slightly during routine activities even on tightly fitted clothing. To eliminate this effect, the coil is stacked on a ground shield layer to suppress the inductor's electric field from entering the body[39].

This approach adds considerable intrinsic capacitance to the resonator (C_R) and decreases the resonant frequency, which reduces the loop's length and thus enhances the ohmic loss and

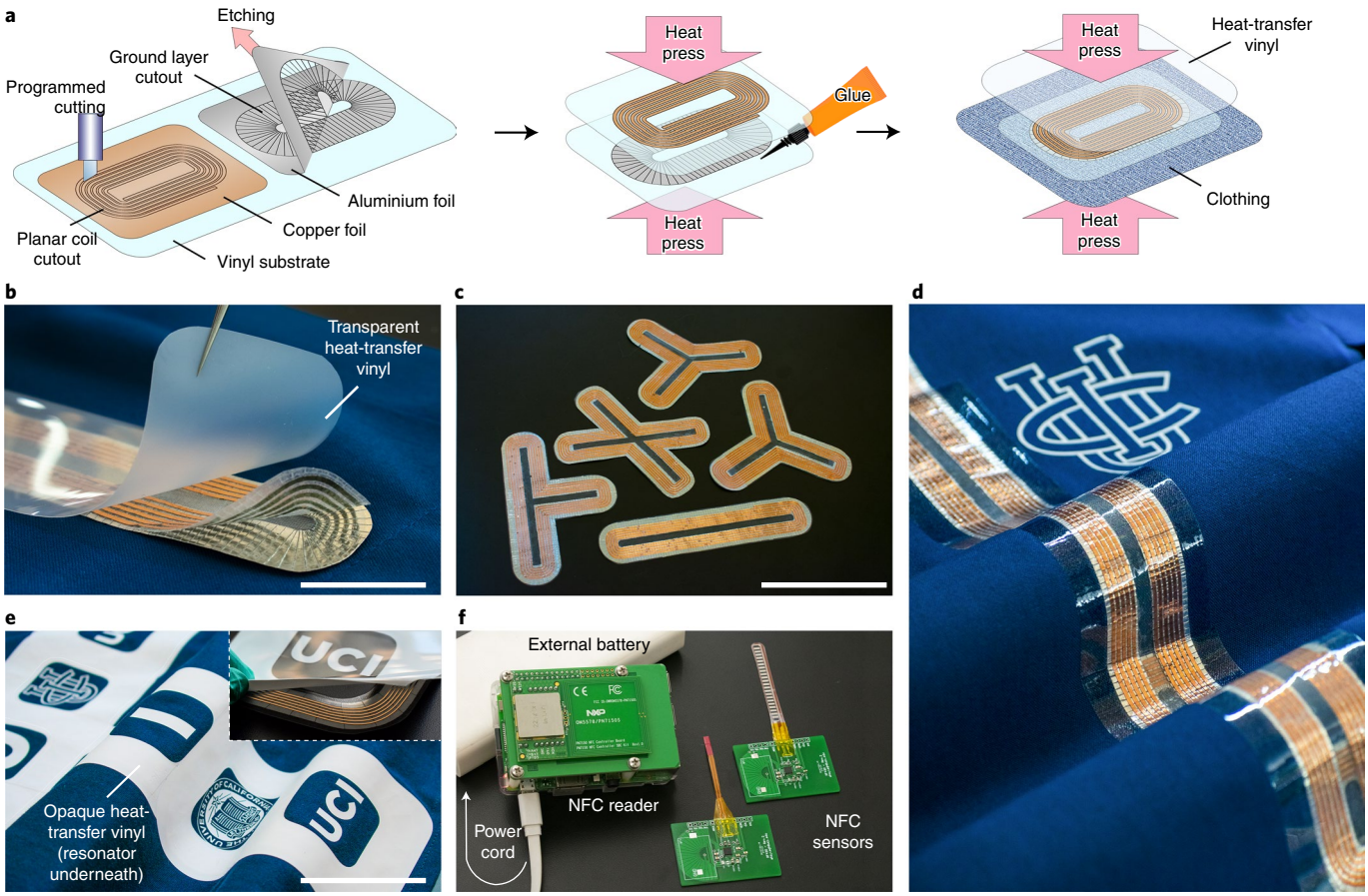

Fig. 3 | Textile-integrated magneto-inductive pathway. a, Resonator fabrication and textile integration steps. **b**, Blow-up image of a resonator showing its stack up (scale bar, 4 cm). **c**, Various designs of flexible resonators for optimal signal transmission and power division (scale bar, 10 cm). **d**, Wearable modular network integrated into the clothing and covered by transparent heat-transfer vinyl as a mechanical fixture (scale bar, 4 cm). **e**, Resonators can be designed to cover wider near-field areas (in this case, using a square element), and can be embedded underneath special coloured vinyl designs (inset). This allows network customizability for both function and style (scale bar, 10 cm). **f**, Battery-free NFC transponders integrated with strain and temperature sensors transferring the respective sensor status to an NFC reader (scale bar, 5 cm).

self-inductance of the resonator (R_R and L_R, respectively). However, this ground layer can induce eddy currents due to its proximity to loop traces. To avoid considerable loss of the resonator's quality factor, we add several slots on the ground layer perpendicular to the loop traces to terminate the eddy currents (Fig. 1a). This compensates for the power dissipation generated from the flow of image currents on the ground layer. Therefore, the slotted ground layer intervenes in between the loop and skin, eliminates the unpredicted spectral shift of the resonator (Fig. 1b), and helps to miniaturize the loop in addition to not largely affecting the resonator's quality factor compared with the case when the loop is directly put on the skin (Supplementary Fig. 1). The magnetic field in this setup is still allowed to flow below and above the resonator despite the presence of this ground layer.

The magneto-inductive waves can propagate through more convoluted pathways involving arrays of magnetically coupled resonators (Fig. 1c). This magnetic connection allows for more flexibility in terms of the resonators' relative placement and introduces a horizontal distance within our network between the reader and sensor nodes (in the x direction), in addition to the vertical distance (VD) between two neighbour nodes (resonator/device) on different pieces of clothing (or the z axis). This network shows the propagation behaviour along the coils (x direction) and typical near-field properties in other directions. Thus, the nodes (including the reader and multiple sensors) in close vicinity of the coil network would be magnetically connected (the network's equivalent circuit comprising N coupled coils plus one reader and sensor with a vertical distance in between is shown in Fig. 1d). Here, resistance, capacitance and self-inductances are represented by R, C and L, respectively. The generator, resonators and devices are shown by indexes g, R and D, respectively. The voltage source V_g originally excites the resonator array.

We assume that the current flowing in the nth resonator has a sinusoidal time dependency with angular frequency ω. Here the resonator coils, each with an impedance of $Z_R = R_R + j\omega L_R + \frac{1}{j\omega C_R}$, are inductively coupled to their closest neighbour resonator with mutual coupling $M_{RR} = k_{RR}L_R$, where M and k represent the mutual inductance and coupling factor, respectively (the indexes RR and DR show inter-resonator and device-resonator relations). The resonators form a linear array with equal distance d_c between two neighbour coils. Here, for simplicity, we start by assuming that the vertical distance is ignorable ($k_{VD} = k_{RR}$). The current running on the nth resonator (ranging from 1 to N) in a linear array can be represented by

$$I_n = I_1 e^{j\phi_1}\, e^{-j\gamma(n-1)d_c}, \quad (1)$$

where γ is the travelling wave's propagation constant and I_1 and Φ_1 are the first loop's current magnitude and phase depending on the excitation (boundary conditions imposed by reader's V_g), respec-

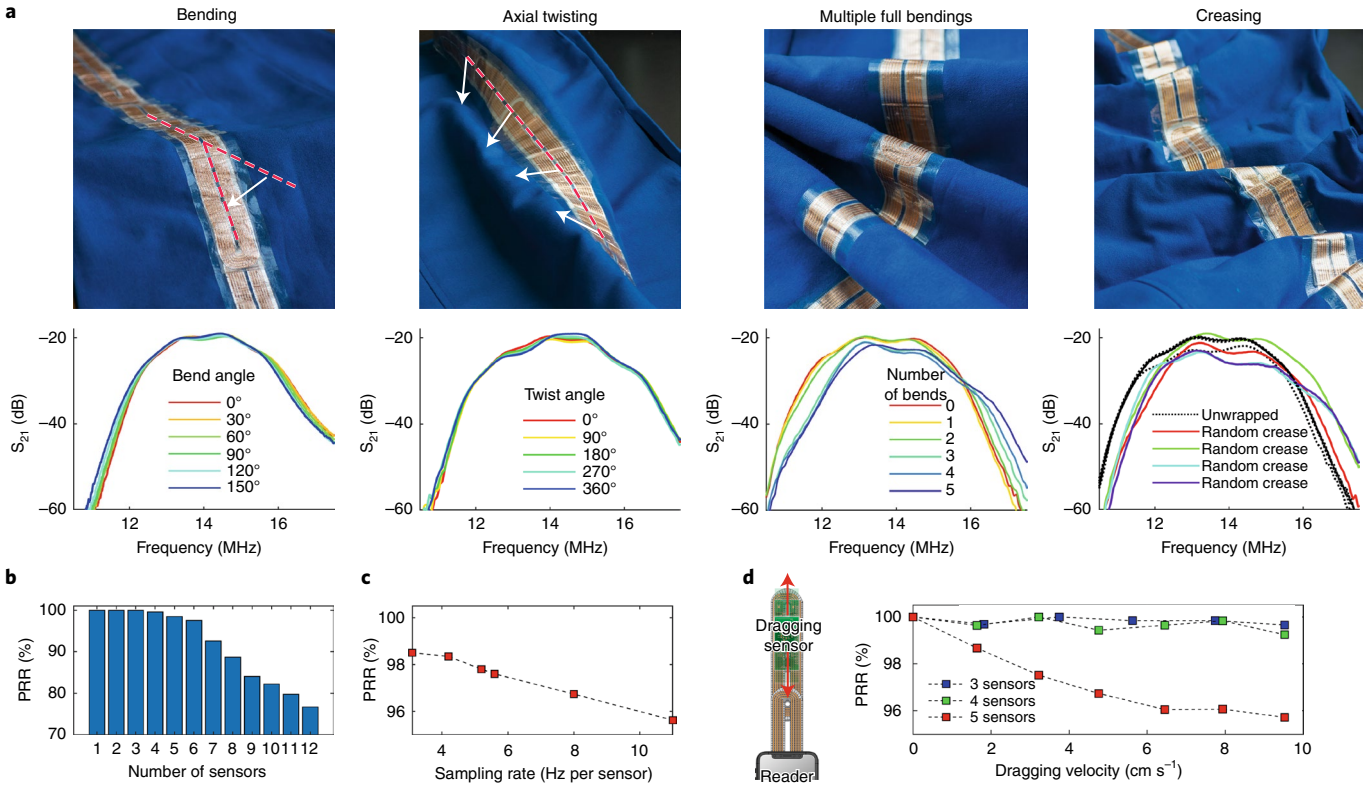

Fig. 4 | Flexible, drag-and-drop NFC networks on textiles. a, Spectral stability of clothing-integrated pathway under mechanical deformations such as bending, axial twisting (per metre length), multiple 360° bendings and repeated creasing/unwrapping. The 80-cm-long deformed inline network passes the transmission and bandwidth requirements enforced by NFC protocols (all scale bars are 10 cm). **b**, Averaged NFC PRR measured for various numbers of sensor transponders along the network with a refresh rate of 5.6 Hz per sensor (and distributed over 1 m of a network). **c**, PRR values for six NFC transponders with various sampling rates. **d**, PRR values for a moving sensor dragged under various velocities along 1 m of the magneto-inductive network for different numbers of sensors under a sampling rate of 9 Hz per sensor.

tively. Kirchhoff's voltage law for the nth coil can be expressed as follows:

$$Z_R I_n + j\omega M_{RR}\left(I_{n-1} + I_{n+1}\right) = 0, \quad (2)$$

which leads to the following dispersion equation.

$$\gamma = \frac{1}{d_c} \times \cos^{-1}\left(\frac{-Z_R}{2j\omega M_{RR}}\right) \quad (3)$$

This structure supports forward and backward travelling waves, thus forming a standing wave along the resonator array. To match the standing wave's spatial harmonics with the array's geometry, we define $\gamma_m = 4\gamma/m$, where m (>1) indicates the number of coils between two spatially equal-phase planes along the standing wave. This enables analysing the propagation characteristics per unit of resonator (instead of length) and would be ultimately helpful to identify the resonator number on which the standing wave's peak is placed. The per-resonator expression of the spatial harmonics facilitates the network's design for the end user to plan the number of resonators on each piece of clothing and thus optimize the BAN. Here $\gamma_m = \beta - j\alpha$ is the harmonic propagation constant (β is the phase and α is the attenuation constant) and is calculated for our typical resonator properties (Fig. 1e).

The propagation constant profile $\beta(\omega)$ may possess different values depending on the coil geometry (reflected in Z_R), coupling factor and harmonic modes (m, which is not necessarily an integer). Dispersion profiles for various modes and electrical properties are compared in Supplementary Fig. 2. We designed and tuned the coils (detailed properties shown in Supplementary Fig. 3) to resonate at the standard frequency (13.56 MHz) of NFC. To afford enough bandwidth for the amplitude-shift keying utilized in NFC protocols, the auxiliary carriers (distanced at 848 kHz from the main carrier at 13.56 MHz) must be covered by the metamaterial's passband. As shown in Fig. 1e, this may be tuned by the inter-resonator coupling (k_{RR}) or equivalently the neighbour-coil distance (d_c). The passband calculations obtained from the dispersion diagrams show that a k_{RR} value of 0.1 is capable of providing sufficient bandwidth for successful long-term communication under varying mechanical distress. This is approximately equivalent to less than 20% neighbour-coil overlap.

Unlike traditional BANs that utilize coils connected by a wire, here the inter-resonator magnetic coupling enables complex network architectures with user-friendly extensions such as inline or fork connections (Fig. 1f). When integrated into clothing, it allows for the BAN's complex signal paths (Fig. 1g) to span across multiple layers of disconnected clothing (for example, from pants to shirts), distinguishing itself from other textile BANs that rely on a wire-based or conductive-thread-based connection.

The VD's effect can be evaluated using circuit theory to calculate the efficiency of the network (Supplementary Fig. 4 shows the equivalent circuit of the resonator chain). First, the transmission (S_{21}) profile of a network (for $N = 11$) without VD is shown (Fig. 2a), where the reader (Tx) and sensor (Rx) at the ends of the inline resonator chain are connected to the first and second ports, respectively. For large enough k_{RR} values, the peak S_{21} (originally centred at 13.56 MHz) splits into N resonances, correlating to the metamaterial passband. This aligns with what is referred to as the

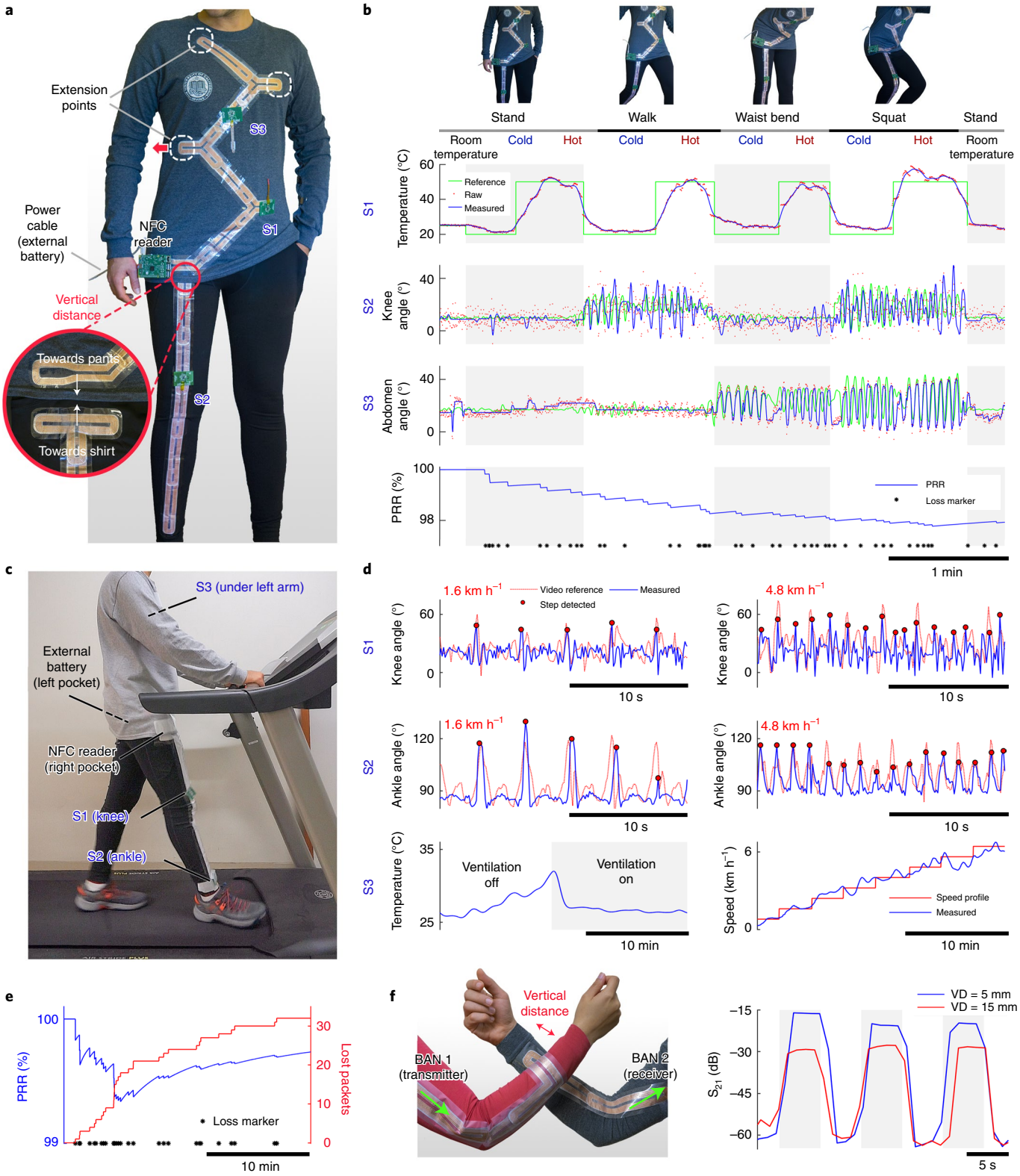

Fig. 5 | Multi-transponder and multiBAN communication by textile-integrated waveguides. a, Shirt and pants on top and underneath the pants/shirt terminals. The NFC reader receives information from multiple sensors and is connected to an external battery. **b**, Real-time, short-term, low-speed monitoring of human activity realized by time-division-based multiple sensor readout within the BAN with a sampling rate of 5.6 Hz per sensor (dots and solid lines show the raw and filtered data, respectively). **c**, High-speed, long-term indoor walk/running activity measurement. The test was performed under a gradually increasing velocity profile for 25 min and BAN was integrated into clothing with coloured vinyl. **d**, Monitoring of sensors during indoor running under various velocity profiles with a sampling rate of 10 Hz per sensor. Steps are detected and marked by circular markers. **e**, Long-term packet-loss monitoring during indoor running. **f**, Body-to-body communication enabled by NFC's plug-and-play characteristics and its measured transmission when dragging the hands close and far over time (comprising an action of a 'digital high-five') for various VD values.

strong coupling of magnetic resonances in the literature. Adding a VD with the coupling factor of k_{VD} at the sixth resonator (middle of the chain) affects the transmission at the central frequency (Fig. 2b). It is shown, however, that the network demonstrates peak transmission performance when $k_{VD} = k_{RR}$. To operate close to this constraint, one may compensate for the low k_{VD} (due to the z-axis distance) by increasing the coil overlap (along the x axis). The S_{21} profile comparison for various VD placements and modulating the VD compensation is shown in Supplementary Fig. 5. Due to the reciprocal nature of the magneto-inductive array, various (single or multiple) VD placements along an inline network may possess similar transmission profiles (Supplementary Fig. 6). This ultimately simplifies spectral optimization and minimizes design rules by enabling the planning of resonator placements before integration into clothing.

According to the benchtop measurement of the inline array of resonators (Fig. 2c) with a fixed Tx and a moving Rx, larger k_{RR} (or smaller d_c) results in an enhanced horizontal range; meanwhile, the S_{21} peak splits (Fig. 2a) and ends up with non-monotonic S_{21} fluctuations along the network. The fluctuations agree well with the envelop of the I_n profile (Supplementary Fig. 2b) and show standing-wave formation. In addition, the wideband spectrum of the transmission (Supplementary Fig. 7) demonstrates the ability to optimize the metamaterial's bandwidth. A small d_c requires a larger number of coils per unit length, eventually increasing the loss at the coil transitions. Although long coils decrease the number of transitions, on the other hand, the number of turns in each coil must be reduced (to maintain the same resonance frequency) and thus both L_R and k_{RR} are lowered, which is not ideal.

The magnetic-field profile simulation in an inline array (with a test VD in the middle) is implemented by the finite element method (Fig. 2d), demonstrating the standing-wave formation and the feasibility of our method for clothing transitions. Powerfully, the approach of magnetically coupled resonators offers in-plane coil rotation (in addition to bending), enabling the creation of various pathway styles including a meandered 'S-shaped' network (Fig. 2e). This allows the magneto-inductive waveguide network to pass through various points on the human body for sensing purposes. The open-ended network may be reformed to a closed loop (Fig. 2f) and allows for reduction in the total number of resonators in the BAN, although it may enforce additional boundary conditions on the network's dispersion and suppress some modes. This concept can be robustly expanded where a pathway branches off from the main signal path (Fig. 2g). Each of the branches can be separately analysed by considering that their first element's current is identical to the main pathway's last element. The experimental transmission profiles of closed-loop and branched network architectures (operating as a magneto-inductive power divider) are quantitatively compared with the straight, undivided pathway. This, in addition to the electrical measurements and simulation of various resonators, is illustrated in Supplementary Fig. 8. The magnetic profiles are simulated for various modes (induced by different coil distances; Supplementary Fig. 9).

To reduce the number of resonant elements, enhance the transmission and achieve higher mechanical flexibility at the network's branched sections, we merged the intersection coils (for example, three coils at the T-shaped junction) into one multi-ended coil. This noticeably reduces the system loss (created primarily by inter-resonators' coupling loss). The reader/network mutual coupling and resonator's ohmic loss, however, yet exist but in lower orders compared with the interconnection attenuation (Fig. 2h).

Clothing integration and multi-sensor studies

An ideally functional BAN should be adaptable to pre-existing clothing and readily expand to the desired body areas based on the user's needs. These should possess a mix-and-match feature in terms of positioning of the network and multiple sensors. Additionally, their functionality should not be limited to only a few hot spots on which the reader/sensor can be placed. Conventional textile BANs, however, usually use a conductive thread sewed on the clothing and are not particularly affordable or easy to fabricate. In addition, these textile networks usually suffer from the inability to cross different pieces of clothing due to their wired nature. Inspired by modern, low-cost, vinyl heat-transfer designs, we address such needs by proposing a facile and versatile technique of integrating metamaterial railways.

The coil trace and slotted ground layer were cut out of copper and aluminium foils, respectively (Fig. 3a). The copper coils minimize the network attenuation and ohmic loss per resonator compared with aluminium (1.5 Ω versus 3 Ω for the design shown in Supplementary Fig. 3), which—in addition to increasing the resonator's quality factor—enhances the network's tolerance for misalignments and possible resonator mistuning. After etching, the layers were first stacked, then placed on the clothing, and finally fixed by heat pressing (Fig. 3b–d). This simple resonator fabrication allows for unique/specialized network designs. For example, wider coils may be utilized to increase the textile area covered by the near-field propagation through the network. In addition to transparent vinyl, coloured opaque vinyl can be used to conceal the BAN and integrate with special vinyl designs, thus embedding NFC transfer capabilities underneath customizable clothing designs (Fig. 3e). The fabrication process is available in Methods. Numerous shirt- and pants-integrated network architectures with transparent and coloured vinyl designs are fabricated (Supplementary Fig. 10), which allow the network architectures to integrate smoothly alongside traditional vinyl T-shirt designs.

The versatility of our network was evaluated by using various readers and sensors (including off-the-shelf chips and an optimized board design) that can be placed close (roughly within a vertical distance of 3 cm) to any point on the resonator chain (Fig. 3f). Our sensor board is based on a commercially available NFC transponder chip integrating an analogue-to-digital converter (ADC) unit that connects to a wide range of analogue sensors, such as strain and temperature sensors (Supplementary Fig. 11). Multiple NFC transponder access and readout were implemented by both an NFC-enabled mobile phone and programmed hardware, as explained in Methods.

Flexibility of the resonator elements exhibiting complex designs is improved by employing thin aluminium, copper and vinyl coatings. Each fabricated resonator element has an overall thickness of about 300 μm and does not impede routine clothing movements. The spectral stability of a resonator array (80 cm long and integrated into cotton clothing) was examined by measuring the transmission (S_{21}) along the two ends of the network under various levels of bending and axial twisting. This shows steady transmission with a minimum bandwidth of 16%. The functionality of the BAN is tested under more severe mechanical deformations such as multiple full (360°) bendings and random creasings. The repeatable stability of the BAN was examined under mechanical distress by creasing at random locations along the network (followed by immediate unwrapping and repeating several times; Fig. 4a).

Here we used a software-based time-domain multiple access (TDMA) approach to achieve switching between the sensing nodes. The controlled surface propagation of magneto-inductive waves eliminates the need for multiple near-field antennas (connected by a wire)[40,41] or complex antenna-switching schemes (needing active microelectronics). This allows conventional NFC-enabled smartphones to operate as compatible readers. The network's wireless efficiency was examined by measuring the NFC packet reception ratio (PRR), defined as the ratio of the number of packets successfully received by the reader to the total number of transmitted packets. Each packet consists of sensor information from all the transponders along the network during one refresh. We note that in practice, however, latency and hysteresis of the strain sensor limit

its performance at higher frequencies (Methods). In addition, the TDMA approach allows up to 12 sensors to be connected along the network. There is a trade-off between the sampling rate, number of sensors and packet loss. The PRR is measured for varying numbers of sensors in reach of the reader (with a sampling rate of 5.6 Hz per sensor), as well as for various sampling rates (with six sensors) in an inline network of an overall length of 100 cm (Fig. 4b,c).

The ability to continuously monitor wireless NFC-enabled devices all along the magneto-inductive resonator railway offers useful applications in unique scenarios such as moving joints within actuators/robotics (which cannot be powered through NFC's regular range) or within highly traceable terminals in gates where multiple objects may move along a local path length (where traditional RF identification would again fail). To validate the drag-and-drop feature of the BAN, we power and probe sensors moving along the network (1 m length) at different velocities and various numbers of sensors within reach. The surface-bound magnetic profile of the planar magneto-inductive array allows for relatively fast sensor dragging with a reliable PRR of above 95% (Fig. 4d).

The upper body part of our studied BAN was designed in a zigzag shape, passing over the abdomen and chest area, although offering the ability to extend the network to the back of the body (potentially interacting with NFC-enabled seats). Similarly, we designed an inline array starting from the hip, passing over the knee and ending by the ankle. The shirt's network ending was designed to overlap with that of the pants within a vertical distance, thus enabling wireless signalling across different pieces of clothing (Fig. 5a). Methods provides detailed sensor placements. The multi-point sensor readout was performed while standing, walking, squatting and waist bending for different temperature zones simulated indoors. All the sensor values were time stamped, transmitted and recorded by the reader at a sampling rate of 5.6 Hz per sensor (equivalent to an overall rate of 16.8 Hz for all the sensors operating together). To minimize the resistive strain and temperature sensor's hysteresis effect and random noises, we applied a data processing algorithm for each sensor value (the processing flow chart is shown in Supplementary Fig. 12). This strategy was implemented in real time and a few seconds after the start of recording (Methods provides the filtering details). This approach effectively achieved steady data with minimal noise fluctuations. The sensors' raw and filtered samples during a short-term exercise (walking for eight steps, six bends and seven squats, each in two different temperature zones) are depicted in Fig. 5b. The cold/hot temperature zones correspond to locally different but close indoor spots generated by a fan/heater (the reference temperature profile is sampled by an infrared thermometer). For applications with conservative power consumption, low-sampling-rate versions of the exercises are performed as well (Supplementary Fig. 13a,b).

To validate the behaviour of the magneto-inductive BAN under longer-term function during more strenuous exercise, we relocated the temperature sensor along the BAN to near the underarm and fixed the sensor's probe on the skin (through a hole on the shirt to capture the core temperature correlate as well). We used a conditional peak detection algorithm to extract the step and pace from the knee and ankle angle information (Fig. 5c,d). The network's PRR was recorded during the activity (Fig. 5e; Methods provides details on the long-term activity validation). The long-term functionality is tested for the lower body part of the network with knee and ankle angles and a temperature sensor (fixed on the skin to capture the skin's surface temperature) during indoor cycling (Supplementary Fig. 13c). Due to the compatibility of the magneto-inductive BAN with the NFC standard, the network operates for a wide range of commercially available NFC-enabled devices (such as smartphones and sensors), with real-time, buffered, offline or cloud-based ecosystems. A sample off-the-shelf NFC ecosystem is integrated into our BAN and tested (Supplementary Fig. 13d).

The surface propagation characteristics of the magneto-inductive structures enable seamless body-to-body communication with no need for terminals. The link is readily established by putting any point of the two contributing BANs close enough (similar to the vertical distance between different pieces of clothing; Fig. 5f and Supplementary Video 1). The external NFC may similarly be generalized to nearby local networks integrated into, for example, driver seats or gateways for monitoring and authentication purposes.

Due to the vinyl sealing of the network, it demonstrates good spectral stability versus wetting. To mimic human sweating (or light raindrops), we added incremental volumes of salty water (a total of 30 ml, with NaCl concentration of 200 mg l^{-1}) on top of the network (covering about 90 cm^2 of the resonators), resulting in a 3% frequency shift and maintaining steady network transmission. Additionally, the textile survived 20 min of handwashing in cold water with stable measured transmission over various washing phases (Supplementary Fig. 14).

The magneto-inductive BAN can be synthesized on demand and at a low cost for personalized wearable networks. This ecosystem can be utilized in various clinical, athletic and daily routines to facilitate real-time healthcare and status monitoring. For instance, integration into patient uniforms in hospitals could allow for seamless patient monitoring where sensors are dragged and dropped across clothing. Professional sports clubs or federations may develop highly customized networks that may be both integrated with their branding and optimized to serve specific needs in athletic training and monitoring. The vinyl-based resonator elements enable users to freely create and readily arrange the network without special equipment, and can be targeted for either local or long-range monitoring along the body. Sensing nodes may be seamlessly swapped or rotated to facilitate plug-and-play measurement of a variety of relevant parameters. Lastly, the magneto-inductive BAN is compared with some recent over-the-air network technologies in Supplementary Table 1.

Conclusions

We have reported a near-field multiBAN system in which wireless sensing nodes can be placed anywhere along the network in a plug-and-play fashion, and the network itself can be designed, built and extended with minimal effort. Our networks offer secure, battery-free, object-to-object and body-to-body transfer of NFC data. The networks are created using a low-cost, rapid prototyping technique of synthesizing textiles functionalized with magneto-inductive waveguides tuned to NFC bands. We expect that the modular nature of this network could allow the concept to be extended in a number of directions. The layer-by-layer conductive vinyl could be readily modified with emerging bio-interactive materials and sensors, and could allow electronic components to be built alongside the body. We also expect the magneto-inductive elements to be scalable to different frequency bands as required by the user, enabling application or person-specific transmission.

Methods

Numerical methods. The equivalent circuit's behaviour was modelled in MATLAB R2020b and validated in Advanced Design System 2020, Keysight. The finite element method simulations of the grounded resonators (including the magnetic-field profile demonstration) were conducted in COMSOL Multiphysics 5.5 (using electromagnetic waves and magnetic-field physics).

Resonator fabrication. The grounded resonators were fabricated by stacking a copper sheet (25 μm thick) on a transparent self-adhesive vinyl-film substrate. Similarly, we used aluminium foil (14 μm thick) for the ground layer. The metal/vinyl layers were stacked on the adhesive cutting mat and cut using a Silhouette Cameo 3 system (Silhouette America). The complementary pattern of the metal foil was etched after cutting. Then, the top aluminium surface of the ground stack was coated with a general-purpose adhesive spray. The coil (copper/vinyl stack) was then aligned and placed on top of the adhesive-coated surface of the ground layer (aluminium/vinyl stack) after one minute. The final stack (copper/vinyl/aluminium/

vinyl) was then immediately covered by inflammable fabric and heat pressed under 260 F for 45 s and allowed to cool afterwards. The adhesive coating should be uniform and controlled to avoid resonance frequency shifts. The resonance behaviour of the grounded coils was then measured (and tuned, if necessary) with a vector network analyser (E5063A, Keysight) linked to a loop antenna via an SMA connector to ensure all the elements resonate at 13.56 MHz to achieve the maximum transmission (a frequency mistuning of about 0.3 MHz was found to be tolerable). The tuning was performed by etching the copper trace (a lower loop length results in lower L_R and C_R, which increases the resonance). Optionally, an additional transparent vinyl layer may be placed on top of the resonator (adhesive facing copper) to seal the resonator and enhance the mechanical and waterproof properties. The ground layer should be of the same shape as the resonating loop and cover its entire area. We added a 1 mm margin to suppress the fringing electric fields (from the resonator to the body) as well. The ground layer's gap distances should be as small as a millimetre to efficiently eliminate eddy currents (Supplementary Fig. 1).

Systematic design procedure of the magneto-inductive network. After designing the resonator such that it resonates at 13.56 MHz, we measured the electrical characteristics (impedance) of the identical resonators and substituted them in our model to find the approximate k_{RR} value based on the dispersion diagrams. For our rectangular coil geometry, $k_{RR} = 0.1$ maps onto 3.2 cm of the neighbour-loop overlap (that is, $d_c = 12$ cm). One may redesign the loop resonator to match a particular clothing shape or application, resulting in a different k_{RR} and thus d_c.

Textile integration. After locating and placing the resonators on top of the clothing, a heat-transfer vinyl (transparent or opaque depending on the design preference) was cut and put on top, and then heat pressed under 300 F for 1 min and allowed to cool afterwards. Cotton clothing is often suggested by vinyl manufacturers due to its tolerance to high temperatures.

NFC sensor transponder. We implemented our sensor ecosystem using ISO15693 sensor transponder RF430FRL152H (Texas Instruments (TI)) with unique identifications, and designed a custom miniature board containing NFC loop antennas (to couple better with our resonators) and analogue sensor-biasing resistors to minimize the ADC gain error. The chips were then programmed over the air to announce the ADC output (known as the sensor value) on the reader's interrogation command under ISO15693. The programming was performed using TI's graphical user interface to interface between the TRF7970A (TI; mounted on MSP430G2553 (TI)) and the transponder chip. We used off-the-shelf strain (short flex sensor, Adafruit Industries) and temperature (CTTS-203856-S02, Amphenol Advanced Sensors) sensors embedded in our transponders. The sampling rate (32 Hz) here is significantly higher in comparison to earlier NFC multiplexing techniques (8 Hz) for a single sensor[12]. The strain sensor (used under 30% strain here, enough to measure knee/ankle bending during activities) showed latency of less than 200 ms, which allowed a sampling rate of 5.6 Hz per sensor. The sampling rates for activity measurement (5.6 Hz per sensor) were set based on the PRR (above 95% for at least five sensors) and the Nyquist sampling theorem (that the sampling rate must be over twice as fast as the activity's highest frequency component, which was estimated to be less than 2.5 cycles or steps per second). The PRR studies (Fig. 4b,c) were run for 10 min (for each number of sensor and each sampling rate) to ensure the PRR values reflect the steady state of the network.

Multi-sensor readout and reliability check. To evaluate the worst-case transmission scenario, any packet with at least one failed sensor data (even if all the other sensor data are successfully delivered) is counted as lost. Our software-based TDMA (integrated into an NFC pathway ecosystem with sensing nodes 1 m away from the central reader) reached a maximum refresh rate of 32 Hz for one sensor, exhibiting a PRR above 98%. This approach allows for a wide array of sensor types used for frequent monitoring. To maintain the same PRR with a larger number of sensors, the sampling rate should be accordingly lowered. We utilized an NXP PN7150 NFC controller shield mounted on a Raspberry Pi system to perform the sensor readout, which broadcasts the reading command along the BAN. To avoid collision among the transponders receiving this command, multiple access with round-robin scheduling was implemented to enable time division between the NFC transponders discovered at the time and looped until receiving the termination command. For sensors with higher readout priority or sampling rate, rate-monotonic scheduling might be beneficial.

Multi-clothing design and sensor placements. Since the network on the pants passes over the pocket, the NFC reader could be placed in the pocket for appropriate excitation, similar to mobile devices routinely placed in pockets. For measuring the pattern of basic human daily activities, we placed two strain sensors at the abdomen area and knee (for bending and pacing recognition) and a temperature sensor above the hip (recording the near-body temperature), with sensing nodes located in the vicinity of the network. The stand-alone reader (placed on the pants pocket) was powered by a wired external battery, and the sensor data were wirelessly streamed to an online cloud platform. Here the co-location of the sensors does not matter as long as they are within the reader's sensitivity range (equivalent to transmission above approximately −35 dB here).

Long-term activity validation. The indoor walk/run was performed under varying speed profiles and a locally controlled ventilation system nearby, and the sensors were probed at a sampling rate of 5.6 Hz per sensor. The knee and ankle angles obtained from the BAN-based measurement were compared with a reference video processing toolbox (video motion capture) to validate the measured actions. The running test was repeated three times (25 min each) under room temperature, in which the ventilation was turned on in the middle of the experiment. Here the core body temperature correlation increased during more strenuous activity, and expectedly reduced (to room temperature) when ventilation was initiated.

Off-the-shelf NFC transponders. The BAN's versatility test was performed using STEVAL-SMARTAG1 NFC transponders. Among the embedded pressure, temperature, humidity and accelerometer sensors, we utilized the accelerometer sensor to detect running while placing the transponder on the ankle. The readout was performed with the ST NFC Sensor application on an Android device.

Verification of activity monitoring. The video tracking of human-activity test subjects was performed using the OpenCV library implemented using Python programming. The measured temperatures were verified with an infrared thermometer. The exercise tests were run by a male human (height, 172 cm; weight, 62 kg).

Real-time sensor data processing. Real-time filtering operates on the basis of the standard deviation (s.d.) of the last four samples (independently for each sensor) and decides to filter or pass the incoming data depending on the fluctuations. The minimum and maximum bounds of the acceptable s.d. are found by the strength of the random noise and extreme fluctuations (such as dropped packet or analogue sensor overflow), respectively. Any sensor values between these boundaries are passed; otherwise, the mean value of the last four samples (including the new sample) is stored to hold the acceptable data. The thresholds vary based on the sensor's noise characteristics and obtained by calibration, and were not altered throughout the experiments.

Data availability

The data that support the plots within this paper and other findings of this study are available from the corresponding author upon reasonable request.

Code availability

The code supporting the NFC readout within this paper is available from the corresponding author upon reasonable request.

Received: 9 March 2021; Accepted: 27 September 2021;
Published online: 11 November 2021

References

1. Yuce, M. R. Wearable sensors get connected with plasmons. *Nat. Electron.* **2**, 217–218 (2019).
2. Kim, J., Campbell, A. S., de Ávila, B. E. F. & Wang, J. Wearable biosensors for healthcare monitoring. *Nat. Biotechnol.* **37**, 389–406 (2019).
3. Yuce, M. R. Implementation of wireless body area networks for healthcare systems. *Sens. Actuator A Phys.* **162**, 116–129 (2010).
4. Kim, H., Hirayama, H., Kim, S., Zhang, R. & Choi, J. Review of near-field wireless power and communication for biomedical applications. *IEEE Access* **5**, 21264–21285 (2017).
5. Ghosh, A., Halder, A. & Dhar, A. S. A variable RF carrier modulation scheme for ultralow power wireless body-area network. *IEEE Syst. J.* **6**, 305–316 (2012).
6. Niu, S. et al. A wireless body area sensor network based on stretchable passive tags. *Nat. Electron.* **2**, 361–368 (2019).
7. Wu, T., Wu, F., Redoute, J. M. & Yuce, M. R. An autonomous wireless body area network implementation towards IoT connected healthcare applications. *IEEE Access* **5**, 11413–11422 (2017).
8. Tian, X. et al. Wireless body sensor networks based on metamaterial textiles. *Nat. Electron.* **2**, 243–251 (2019).
9. Tian, X., Yang, X. and Ho, J. S. Energy-efficient and secure wireless body sensor networks with metamaterial textiles. In *2019 IEEE Biomedical Circuits and Systems Conference (BioCAS)* 1–4 (IEEE, 2019). https://doi.org/10.1109/BIOCAS.2019.8919179
10. La, Q. D. et al. Dense deployment of BLE-based body area networks: a coexistence study. *IEEE Trans. Green Commun. Netw.* **2**, 972–981 (2018).
11. Kianinejad, A., Chen, Z. N. & Qiu, C. Low-loss spoof surface plasmon slow-wave transmission lines with compact transition and high isolation. *IEEE Trans. Microw. Theory Tech.* **64**, 3078–3086 (2016).
12. Lin, R. et al. Wireless battery-free body sensor networks using near-field-enabled clothing. *Nat. Commun.* **11**, 444 (2020).
13. Dautta, M. et al. Wireless Qi-powered, multinodal and multisensory body area network for mobile health. *IEEE Internet Things J.* **8**, 7600–7609 (2020). https://doi.org/10.1109/JIOT.2020.3040713

14. Xu, L. et al. Characterization and modeling of embroidered NFC coil antennas for wearable applications. *IEEE Sens. J.* **20**, 14501–14513 (2020).
15. Masuda, Y., Noda, A. & Shinoda, H. Body sensor networks powered by an NFC-coupled smartphone in the pocket. *In 2018 40th Annual International Conference of the IEEE Engineering in Medicine and Biology Society (EMBC)* **2018**, 5394–5397 (2018).
16. Mishra, V. & Kiourti, A. Wearable magnetoinductive waveguide for low-loss wireless body area networks. *IEEE Trans. Antennas Propag.* **69**, 2864–2876 (2021).
17. Huang, P. S. W. NFC antenna for wearable application. US patent US9998182B2 (2018).
18. Koshiji, F., Fujita, Y. and Koshiji, K. Wireless body area network using magnetically-coupled wearable coils. In *2015 IEEE CPMT Symposium Japan (ICSJ)* 208–211 (IEEE, 2015). https://doi.org/10.1109/ICSJ.2015.7357399
19. Das, D., Maity, S., Chatterjee, B. & Sen, S. *Enabling Covert Body Area Network using Electro-Quasistatic Human Body Communication* (Springer, 2019).
20. Zhong, W., Lee, C. K. & Ron Hui, S. Y. General analysis on the use of Tesla's resonators in domino forms for wireless power transfer. *IEEE Trans. Ind. Electron.* **60**, 261–270 (2013).
21. Wang, B., Yerazunis, W. & Teo, K. H. Wireless power transfer: metamaterials and array of coupled resonators. *Proc. IEEE* **101**, 1359–1368 (2013).
22. Stevens, C. J., Chan, C. W. T., Stamatis, K. & Edwards, D. J. Magnetic metamaterials as 1-D data transfer channels: an application for magneto-inductive waves. *IEEE Trans. Microw. Theory Tech.* **58**, 1248–1256 (2010).
23. Solymar, L. & Shamonina, E. *Waves in Metamaterials.* https://doi.org/10.1080/00107511003790480 (OUP Oxford, 2009).
24. Sydoruk, O., Zhuromskyy, O., Shamonina, E. & Solymar, L. Phonon-like dispersion curves of magnetoinductive waves. *Appl. Phys. Lett.* **87**, 072501 (2005).
25. Syms, R. R. A., Shamonina, E., Kalinin, V. & Solymar, L. A theory of metamaterials based on periodically loaded transmission lines: interaction between magnetoinductive and electromagnetic waves. *J. Appl. Phys.* **97**, 064909 (2005).
26. Xu, Z., Shi, J., Davis, R. J., Yin, X. & Sievenpiper, D. F. Rainbow trapping with long oscillation lifetimes in gradient magnetoinductive metasurfaces. *Phys. Rev. Appl.* **12**, 024043 (2019).
27. Stevens, C. J. Magnetoinductive waves and wireless power transfer. *IEEE Trans. Power Electron.* **30**, 6182–6190 (2015).
28. Huang, S. D., Li, Z. Q. and Li, Y. Transfer efficiency analysis of magnetic resonance wireless power transfer with intermediate resonant coil. *J. Appl. Phys.* **115**, 17A336 (2014).
29. Zhang, F. et al. Relay effect of wireless power transfer using strongly coupled magnetic resonances. *IEEE Trans. Magn.* **47**, 1478–1481 (2011).
30. Zhong, W. X., Lee, C. K. & Hui, S. Y. R. Wireless power domino-resonator systems with noncoaxial axes and circular structures. *IEEE Trans. Power Electron.* **27**, 4750–4762 (2012).
31. Puccetti, G., Reggiani, U. & Sandrolini, L. Experimental analysis of wireless power transmission with spiral resonators. *Energies* **6**, 5887–5896 (2013).
32. Olenik, S., Lee, H. S. & Güder, F. The future of near-field communication-based wireless sensing. *Nat. Rev. Mater.* **6**, 286–288 (2021). https://doi.org/10.1038/s41578-021-00299-8
33. Atanasova, G. & Atanasov, N. Small antennas for wearable sensor networks: impact of the electromagnetic properties of the textiles on antenna performance. *Sensors* **20**, 5157 (2020).
34. Taparugssanagorn, A., Pomalaza-Ráez, C., Tesi, R., Hamalainen, M. & Iinatti, J. Effect of body motion and the type of antenna on the measured UWB channel characteristics in medical applications of wireless body area networks. In *2009 IEEE International Conference on Ultra-Wideband* 332–336 (IEEE, 2009).
35. Fortino, G., Giannantonio, R., Gravina, R., Kuryloski, P. & Jafari, R. Enabling effective programming and flexible management of efficient body sensor network applications. *IEEE Trans. Human-Mach. Syst.* **43**, 115–133 (2013).
36. Gravina, R., Alinia, P., Ghasemzadeh, H. & Fortino, G. Multi-sensor fusion in body sensor networks: state-of-the-art and research challenges. *Inf. Fusion* **35**, 68–80 (2017).
37. Arab Hassani, F. et al. Smart materials for smart healthcare—moving from sensors and actuators to self-sustained nanoenergy nanosystems. *Smart Mater. Med.* **1**, 92–124 (2020).
38. Shamonina, E., Kalinin, V. A., Ringhofer, K. H. & Solymar, L. Magnetoinductive waves in one, two, and three dimensions. *J. Appl. Phys.* **92**, 6252 (2002).
39. Yue, C. P. & Wong, S. S. On-chip spiral inductors with patterned ground shields for Si-based RF ICs. *IEEE J. Solid-State Circuits* **33**, 743–752 (2003).
40. Aslanidis, K. and Gunasegaran, V. N. *TRF7970A NFC Reader Antenna Multiplexing*. Report No. SLOA231 (Texas Instruments, 2016). https://www.ti.com/lit/an/sloa231/sloa231.pdf?ts=1623371911451
41. Wyatt, J. *TRF7960A RFID Multiplexer Example System*. Report No. SLOA167 (Texas Instruments, 2012). https://www.ti.com/lit/an/sloa167/sloa167.pdf?ts=1621460422412

Acknowledgements

This work was supported by faculty startup granted by the University of California, Irvine, and was partially supported by the National Science Foundation through grant CBET-1928326, as well as the CAREER award through ECCS-1942364 received by P.T., and ECCS-2028782 received by F.K.

Author contributions

A.H. and P.T. planned and conceptualized the study. A.H. conducted the theoretical studies and simulations. A.H., A.H.A.Z. and M.D. performed the experiments. A.H.A.Z., A.H. and A.J. developed the hardware. M.D. and F.K. commented on the manuscript. A.H. and P.T. wrote the manuscript.

Competing interests

The authors declare no competing interests.

Additional information

Supplementary information The online version contains supplementary material available at https://doi.org/10.1038/s41928-021-00663-0.

Correspondence and requests for materials should be addressed to Peter Tseng.

Peer review information *Nature Electronics* thanks John Ho and Jeonghyun Kim for their contribution to the peer review of this work.

Reprints and permissions information is available at www.nature.com/reprints.

Publisher's note Springer Nature remains neutral with regard to jurisdictional claims in published maps and institutional affiliations.